ANALYSIS OF SPECTRA OF SOLAR WIND MAGNETIC FIELD COMPONENTS FLUCTUATIONS ACROSS FAST REVERSE INTERPLANETARY SHOCKS

© 2025 O. V. Sapunova*, N. L. Borodkova, Yu. I. Yermolaev***, G. N. Zastenker****

Space Research Institute, Russian Academy of Sciences, Moscow, Russia

**e-mail: sapunova_olga@cosmos.ru*

***e-mail: borodkova_nl@cosmos.ru*

****e-mail: yermol@cosmos.ru*

*****e-mail: gzastenk@iki.rssi.ru*

Received March 13, 2025

Revised April 16, 2025

Accepted May 22, 2025

Abstract. Fluctuations in the values of interplanetary magnetic field components of the solar wind plasma near the front of a fast reverse shock were considered according to data from the WIND satellite with a time resolution of 11 Hz. Two options for dividing the magnetic field vector into components were considered: according to the GSE coordinate system and relative to the normal of the front of the interplanetary shock. It was found that for the upstream region of the solar wind, the break frequency of the spectrum of magnetic field components fluctuations lies in the frequency range from 0.37 to 1.37 Hz. For the downstream region of the solar wind, the break frequency shifts to the range from 0.45 to 1.58 Hz, which corresponds to the scale of the proton inertial length. It has been shown that the slope of the fluctuations spectra of the interplanetary magnetic field components varies both on MHD and transient scales, although to varying degrees. At transition scales, the difference can be significant.

Keywords: *solar wind, plasma, magnetic field, turbulence, power spectra, interplanetary shock*

DOI: 10.31857/S00167940250505e1

1. INTRODUCTION

Interplanetary shock waves (ISWs) are of considerable interest to study both as a carrier of perturbations from the Sun to the Earth and in terms of solar wind (SW) energy redistribution on different scales of plasma turbulence [Bruno and Carbone, 2013; Kolmogorov, 1962; Leamon et al.,

2000]. At the front of the interplanetary shock wave, there is an abrupt change in the solar wind plasma parameters and the interplanetary magnetic field. Various wave phenomena can be observed near the front, for example, tsunamis of oscillations (both leading and lagging) of both the interplanetary magnetic field and solar wind plasma parameters. The jump itself is called a shock wave ramp. The ramp is a thin transition layer from unperturbed to perturbed solar wind, in which the processes of redistribution of the energy of the directed motion of the plasma into thermal energy and acceleration of particles to high energies on scales of the order of a few values of the ion inertial length occur

The energy of the solar wind system is believed to be in structures with scales~ of 10^6km or more and is transferred to smaller scales through a cascade of turbulent fluctuations. At scales on the order of the proton gyroradius (~10^3 km), kinetic processes begin to play an important role, energy dissipation occurs, and, as a consequence, plasma heating occurs [Matthaeus et al., 2016]. Since wave processes favoring energy redistribution take place at and near the front of the ICE, the study of the influence of the ICE on the plasma turbulence characteristics is of great importance.

Interplanetary shock waves can be divided into different groups based on a number of attributes, including classification by fast/slow and forward/reverse type: fast forward (FF), fast reverse (FR), slow forward (SF), and slow reverse (SR) [Oliveira, 2017] - see Fig. 1.

Fig. 1.

For interplanetary shock waves of the "fast straight line - FF" type, many studies have been carried out to investigate the power spectrum of magnetic field fluctuations, e.g., [Pitňa et al., 2021]. In particular, it has been shown that the power spectrum shape (PSD) is similar for the perturbed and unperturbed regions, although the total power spectrum can increase significantly in the perturbed region. Similar results, indicating that the power of magnetic field fluctuations increases in the transition from the unperturbed to the perturbed region of the NE flow as the front crosses the direct MUV front, are presented in [Zhao et al., 2021]. However, other types of shock waves are much less frequently considered [Park et al., 2023].

This paper is devoted to the study of the second most common type of MUVs, "fast inverse - FR". We calculated the slope coefficient of the power spectrum of magnetic field fluctuations and its components in both the perturbed and unperturbed regions of the fast inverse MUV. The slope coefficient was calculated separately for the MHD region of the spectrum and for the transition region.

One of the parameters investigated in this work was the position of the kink in the fluctuation spectrum, which shows the transition from MHD scales and is determined by the processes responsible for energy dissipation in the plasma. Depending on which process prevails and is leading

for a given set of parameters, the position of the kink can correspond, for example, to the proton inertial length L (fluctuations are determined by energy transfer between thin current layers, [Leamon et al., 2000; Smith et al., 2001]) or the proton gyroradius R (fluctuations are determined by a cascade of Alfvénian fluctuations, [Howes et al., 2008; Schekochihin et al., 2009]). The frequency determined by the inertial length of the ion:

$$F_L = V/2\pi L, \quad (1)$$

where V is the plasma streaming velocity; $L = c/\omega_i$ is the inertial length of the ion (c is the speed of light); $\omega_i = (4\pi n_i/m_i)^{1/2}$ is the plasma frequency of the ion; n_i is the ion concentration; m_i is the mass of the ion.

In this study, we divided the fluctuation spectrum at the frequency corresponding to the inertial length of the proton. However, the frequency correlated with the gyroradius of the proton was also specified.

2. DATA USED AND PROCESSING METHODOLOGY

The data of the MFI magnetometer [Lepping et al., 1995] installed on the WIND satellite - the module and components of the interplanetary magnetic field (IMF) with an interrogation frequency of 11 Hz were used in this work. Plasma parameters such as velocity, temperature, and solar wind concentration were determined using data from the SWE [Ogilvie et al., 1995] and 3DP [Lin et al., 1995] instruments of the same satellite. The SWE and 3DP instruments measure ion energy spectra with 92 and 3 s resolution, respectively. The 3DP instrument has the best temporal resolution, but it has operating intervals for which its data are not reliable and are highly underestimated, such as the proton concentration. This can give an error in determining the fracture frequency, so additionally the measurement data from the SWE instrument were used.

Fig. 2.

An example of a fast backward interplanetary shock wave registered on March 20, 2021 at 11:16 UT on the WIND satellite is shown in Fig. 2. As can be seen from the figure, all parameters decrease at the front of such an ICE, except for the NE velocity. The concentration of solar wind protons fell from 9.7 to 3.1 cm^{-3}; the temperature fell from 60 to 28 eV, and the velocity increased from 545 to 651 km/s. The magnetic field modulus also decreased from 11.1 to 5.3 nTL. Thus, the event was classified as a reverse shock wave. The propagation velocity of the reverse shock wave V_{IP} was 303 km/s. The ratio of gas pressure to magnetic pressure (parameter β) for this event was 1.2, indicating an approximate equality of magnetic and thermal pressures. At the same time, the magnetosonic Mach number was 3.2, which can be called an average value for FR-type MUVs (more

details in paragraph 3). The angle between the direction of the magnetic field vector in front of the front and the normal to the wave front (θ_{Bn}) was 31°, which means a quasi-parallel shock wave.

To construct the fluctuation spectra, we took intervals of interplanetary magnetic field measurements lasting 50 min before/after the shock front crossing. To exclude the influence of subtle structures (e.g., tsunamis) associated directly with the ramp (parameter jump), we took a 5 min interval. The component under consideration was normalized to the mean value during this interval. The spectra were read using the fast Fourier transform. The obtained frequency spectra were smoothed by window filtering in the frequency space (Hamming windows were used). The maximum frequency of the range over which the slope of the transition region was calculated was 2.5 Hz to exclude noise near high frequencies.

A total of 38 fast backward interplanetary shock waves recorded by the WIND satellite were considered. Table 1 presents the calculated front parameters of these MUVs. The number of shock waves used for statistical analysis can be increased in future works with further data processing.

Table 1.

3. RESULTS

3.1. Statistics of changes in solar wind parameters and classifying parameters

The statistics of the variation of the plasma and magnetic field parameters at the reverse MUV front, as well as the classifying parameters, are shown in Fig. 3 and Fig. 4. In Fig. 3, it can be seen that the average ratio of the magnitude of the magnetic field modulus in the perturbed region to the unperturbed region is 1.9, and the whole range is from 1 to 3. The proton concentration in the perturbed region rarely increases by more than a factor of 2.5, with an average value of 2.1. At the reverse MUVs, the proton temperature increased at most by a factor of 2.6. The jump in the transport velocity (*delta V*) for fast reverse shock waves only exceeded 120 km/s in 2 events. For comparison, in the case of fast direct MIEs, large changes in the parameters are characteristic: the jump in the transport velocity up to 280 km/s, the ratio of the temperature in the perturbed region to the unperturbed region up to 7, and the concentration ratio up to the maximum possible 4.

Fig. 3.

Fig. 4.

Fig. 4 gives the statistics of the classifying parameters of fast inverse MUVs. The parameter β is generally small, averaging 0.9, and most of the events have a parameter β not exceeding 1.5. The exception was an event where the parameter beta was found to be 4.5. The parameter θ_{Bn} indicates

that most of the MUVs considered were either quasiperpendicular or oblique. The magnetosonic Mach number M_{ms} for the backward waves in the sample ranged from 1 to 8.4.

Statistics of changes in plasma parameters and classification parameters for fast shock waves were presented in our previous work [Sapunova et al., 2024].

3.2. Power spectra of fluctuations

An example of the fluctuation power spectra for the fast inverse MUV recorded on 20.03.2021 is shown in Fig. 5 and Fig. 6. The power spectra of fluctuations of the interplanetary magnetic field components are presented for two decomposition variants - along the axes of the GSE coordinate system and with respect to the normal of the MUV front - parallel and perpendicular (given from left to right, respectively). The spectra are given for the unperturbed (Fig. 5) and perturbed regions (Fig. 6).

Fig. 5.

Fig. 6.

We can see an increase in the power of fluctuations when moving to the perturbed region, which is fully consistent with both theoretical representations and previous work [Park et al., 2023]. *The* frequency $F_L$increases behind the interplanetary shock front from 0.8 to 1.2 Hz. It follows from formula (1) that the velocity in the perturbed region is smaller and the concentration is larger than in the unperturbed region. The final effect on the frequency change is determined more by the concentration, although it enters the formula to the extent of ½. However, the decrease in the transport velocity modulus is usually of the order of 10-20% of the value in the undisturbed region, while the concentration can increase by a factor of several (but no more than 4).

The slope coefficient K in the MHD region changes little - it is equal to -1.7 for most spectra, with some exceptions. The only spectrum with stronger tilting is the spectrum of the B_Z component in the unperturbed region. However, when considering the transition region of the spectra, a significant difference in the slopes in the transition from the unperturbed to the perturbed solar wind is noticeable. The slope becomes much more gentle for the perturbed region, most strongly in this event for the B_X and B_Z components, from -4.0 to -3.1 and from -3.3 to -2.6, respectively. The slope for the decay components along/perpendicular to the normal to the MUV front changed less, but for the perpendicular component the change was 0.4.

All 38 intersections of fast inverse MUVs were processed using this technique. Histograms of the distribution of the counted parameters - the frequency of breaks in the spectra of fluctuations of

the interplanetary magnetic field components - were plotted using the obtained data.

3.3. Statistics of the slope of the fluctuation power spectra

Fig. 7 and Fig. 8 show the statistics of the change in the slope of the power spectrum in the case of a fast inverse MUV. In Fig. 7 presents the slope statistics for the MHD region, and Fig. 8 presents the slope statistics for the transient region of the spectrum.

Fig. 7.

Fig. 8.

From the magnetic field measurements, it can be observed that in the MHD part of the spectrum, the slope can be steeper in the unperturbed region. This observation is consistent with the results obtained in [Park et al., 2023]. We observe this effect for all components in both decompositions of the magnetic field vector (B_X, B_Y, B_Z, $B_\parallel$, $B_\perp$). The mean value does not change much, but rather the shape of the distribution changes - in the unperturbed region it has a wider range. This observation can be explained by the energy transfer to smaller scales of fluctuations, which is also consistent with some observations that will be described below - for the transient region of the spectrum.

Fig. 8 shows the histograms of the distribution of the slope coefficients of the fluctuation power spectrum for the transient part of the spectrum in the unperturbed and perturbed regions.

The slope of the spectrum in the transition region is noticeably steeper than in the MHD region, which is consistent with the previously listed works on power spectra. At the same time, the unperturbed region is characterized by a steeper slope of the transition part of the spectrum than in the perturbed region of the solar wind. This observation is explained by the redistribution of energy from the MHD scales to the transition region and then to the kinetic region. The width of the distribution also changes - in the unperturbed solar wind the slope range is wider than in the perturbed one. The average value of the slope in the unperturbed wind for the components B_X, B_Y, B_Z is respectively: -3.37, -3.15, -3.40, and in the perturbed one: -2.82, -2.76, -2.59. For the decomposition with respect to the normal to the MUV front, we also observe a steeper slope in the unperturbed region of the solar wind, and a more gentle slope in the perturbed region, with increasing range of the distribution.

4. DISCUSSION AND CONCLUSIONS

Power spectra of the modulus fluctuations and interplanetary magnetic field components in the perturbed and unperturbed region (before and after the front) for 38 fast reverse shock waves were

obtained from the MFI magnetometer measurements on the WIND satellite. For each spectrum, the slopes of the MHD and transition parts of the spectrum, as well as the position of the break frequency between the parts of the spectrum, were determined.

It was obtained that the kink frequency of the spectra lies in the range from 0.37 to 1.37 Hz in the unperturbed region for the reverse shock wave and from 0.45 to 1.58 Hz in the perturbed region. The mean values were 0.72 and 0.92 Hz, respectively. The frequency increase in the perturbed region is due to an increase in the concentration behind the reverse shock front.

According to measurements of the interplanetary magnetic field, it is shown that after the passage of a fast reverse shock wave, the MHD part of the spectrum changes little, the average value of the slope fluctuates insignificantly, but the shape of the distribution changes - in the perturbed region of the solar wind, the frequency range of the kink becomes narrower.

It should be noted that the transition region of the fluctuation spectrum has a much larger slope, which was absolutely expected. The magnitude of the change at the crossing of the shock front can be quite significant - up to 0.9. The range of values of the slope of this part of the spectrum obtained for the components B_X, B_Y, B_Z turned out to be wider than the similar range calculated for the components $B_\parallel$, $B_\perp$. Nevertheless, the behavior of the distribution at the crossing of the MCE front is similar - the spectrum in the transition region becomes more gentle. This observation is consistent with earlier results [Ryazantseva et al., 2020]. Further work will be devoted to increasing the statistics and clarifying the influence of cyclotron frequency on the shape of the spectrum.

ACKNOWLEDGEMENTS

The authors thank NASA CDAWEB for the opportunity to use the plasma and magnetic field parameter data measured on the WIND satellite.

FUNDING

The work was performed within the framework of the State Assignment of the Space Research Institute of the Russian Academy of Sciences on the topic PLASMA.

REFERENCES

1. *Ryazantseva M.O., Rakhmanova L.S., Ermolaev Yu.I., Lodkina I.G., Zastenker G.N., Chesalin L.S.* Characteristics of the turbulent flow of the solar wind in plasma compression regions // Space Research. V. 58. No. 6. P. 503-512. 2020. https://doi.org/10.31857/S0023420620060096

2. *Sapunova O.V., Borodkova N.L., Zastenker G.N.* Analysis of the spectra of fluctuations in the magnitude of the plasma flux and the magnetic field modulus on reverse shock waves // Solar-terrestrial Physics. V. 10. No. 3. P. 62-69. 2024. https://doi.org/10.12737/szf-103202407
3. *Bruno R., Carbone V.* The solar wind as a turbulence laboratory // Living Rev. Solar Phys. V. 10. N 1. ID 2. 2013. https://doi.org/10.12942/lrsp-2013-2
4. *Howes G.G., Cowley S.C., Dorland W., Hammett G.W., Quataert E., Schekochihin A.A.* A model of turbulence in magnetized plasmas: Implications for the dissipation range in the solar wind // J. Geophys. Res. – Space. V. 113. N 5. ID A05103. 2008. https://doi.org/10.1029/2007JA012665
5. *Kolmogorov A.N.* A refinement of previous hypotheses concerning the local structure of turbulence in a viscous incompressible fluid at high Reynolds number // J. Fluid Mech. V. 13. N 1. P. 82–85. 1962. https://doi.org/10.1017/S0022112062000518
6. *Leamon R.J., Matthaeus W.H., Smith C.W., Zank G.P., Mullan D.J., Oughton S.* MHD-driven kinetic dissipation in the solar wind and corona // Astrophys. J. V. 537. N 2. P. 1054–1062. 2000. https://doi.org/10.1086/309059
7. *Leppin R P., Acũna M.H., Burlaga L.F. et al.* The WIND magnetic field investigation // Space Sci. Rev. V. 71. N 1–4. P. 207–229. 1995. https://doi.org/10.1007/BF00751330
8. *Lin R.P., Anderson K.A., Ashford S. et al.* A three-dimensional plasma and energetic particle experiment for the WIND spacecraft // Space Sci. Rev. V. 71. N 1–4. P. 125–153. 1995. https://doi.org/10.1007/BF00751328
9. *Matthaeus W.H., Weygand J.M., Dasso S.* Ensemble space-time correlation of plasma turbulence in the solar wind // Phys. Rev. Lett. V. 116. ID 245101. 2016. https://doi.org/10.1103/PhysRevLett.116.245101
10. *Ogilvie K.W., Chornay D.J., Fritzenreiter R.J. et al.* SWE, a comprehensive plasma instrument for the Wind spacecraft // Space Sci. Rev. V. 71. N 1–4. P. 55–77. 1995. https://doi.org/10.1007/BF00751326
11. *Oliveira D.M.* Magnetohydrodynamic shocks in the interplanetary space: a theoretical review // Braz. J. Phys. V. 47. N 1. P. 81–95. 2017. https://doi.org/10.1007/s13538-016-0472-x
12. *Park B., Pitňa A., Šafránková J., Němeček Z., Krupařová O., Krupař V., Zhao L., Silwal A.* Change of spectral properties of magnetic field fluctuations across different types of interplanetary shocks // Astrophys. J. Lett. V. 954. N 2. ID 51. 2023. https://doi.org/10.3847/2041-8213/acf4ff
13. *Pitňa A., Šafránková J., Němeček Z., Ďurovcová T., Kis A.* Turbulence upstream and downstream of interplanetary shocks // Front. Phys. V. 8. ID 626768. 2021. https://doi.org/10.3389/fphy.2020.626768
14. *Schekochihin A.A., Cowley S.C., Dorland W., Hammett G.W., Howes G.G., Quataert E., Tatsuno T.* Astrophysical gyrokinetics: kinetic and fluid turbulent cascades in magnetized weakly

collisional plasmas // Astrophys. J. Suppl. S. V. 182. N 1. P. 310–377. 2009. https://doi.org/10.1088/0067-0049/182/1/310
15. *Smith C.W., Mullan D.J., Ness N.F., Skoug R.M., Steinberg J.* Day the solar wind almost disappeared: Magnetic field fluctuations, wave refraction and dissipation // J. Geophys. Res. – Space. V. 106. N 9. P. 18625–18634. 2001. https://doi.org/10.1029/2001JA000022
16. *Zhao L.-L., Zank G.P., He J.S. et al.* Turbulence and wave transmission at an ICME-driven shock observed by the Solar Orbiter and Wind // Astron. Astrophys. V. 656. ID A3. 2021. https://doi.org/10.1051/0004-6361/202140450

Table 1. Key characteristics of the fast inverse MUVs discussed in the paper. B_d/B_u, N_d/N_u, T_d/T_u – ratio of values in the perturbed region to the value in the unperturbed region: magnetic field modulus, concentration, and temperature; *delta V* - difference in the transport velocity before and after the ramp. V_{IP} is the shock propagation velocity, θ_{Bn} is the angle between the normal to the MUV front and the magnetic field vector in the undisturbed region, M_{ms} is the magnetosonic Mach number, β is the beta parameter (ratio of thermal pressure to magnetic pressure in the undisturbed region).

Date	Time	B_d/B_u	N_d/N_u	T_d/T_u	*delta V* km/s	V_{IP} km/s	$\theta_{(Bn)}$ deg	M_{ms}	β
05.04.2005	2:55:11	2	2.7	2.3	67.7	473	78.5	4.2	0.6
08.05.2005	17:01:02	1.8	1.8	1.9	66.5	444.5	58.7	3.7	1.3
22.08.2006	16:48:02	1.4	1.8	1	34.8	352.9	49.9	5.3	0.4
24.09.2006	6:17:17	2	3.8	2.1	142	387.2	57.4	4.2	0.4
01.10.2006	8:57:44	2.3	3.3	1.5	68.6	277.2	76.1	2.8	0.5
07.10.2006	20:08:11	1.7	2	1.5	57.5	373.3	87	4.8	1.1
10.11.2006	10:02:59	1.8	1.6	1.5	34.3	233.4	48.9	1.9	0.7
10.08.2008	3:50:50	2.1	2.8	2.5	79.8	285.9	59	3.6	1.2
22.07.2009	10:30:32	1.7	1.9	1.1	57.6	336.6	65.8	3.7	0.9
10.09.2011	22:01:07	1.8	2.3	2.2	89.9	342	72.7	3.9	0.7
25.10.2011	17:09:32	1.6	1.7	1.6	47.2	432	11	3.6	0.1
24.03.2012	11:07:56	2.2	1.9	1.9	55.4	380	80.1	5.4	0.5
13.04.2012	8:30:57	1.5	1.6	1.7	39.1	251	17.8	1.9	4.5
30.06.2012	16:34:59	1.5	2.1	1.7	28.7	267.1	62.5	3.1	1.1
13.10.2012	16:09:14	1.6	1.8	1.4	56.3	450.8	76	5.3	0.8
26.01.2013	21:16:23	2.8	2.3	1.7	94.2	346.5	57.8	3.8	1.4
02.06.2013	2:33:14	2.7	2.4	1.3	106.3	409.7	73.2	3.5	1.2
26.07.2013	3:19:36	1.6	1.4	1.6	38	312	87.1	3.9	2
09.11.2013	15:23:55	2.2	1.8	1.5	82.3	255.4	82.7	2.6	1.2
08.12.2013	7:31:50	1.9	2.5	2.6	140	344.4	59.7	3.5	1
14.01.2014	7:39:08	1.5	1.7	1.6	26.4	491.4	45.3	5	0.3
17.02.2014	5:34:50	1.8	1.4	1	35.5	55.9	81.8	0.6	0.1
21.06.2014	7:45:47	1.9	2.1	1.6	40	314.6	17.7	4.4	0.3
13.05.2015	9:58:20	2.6	2.2	1.6	92.1	328	22.6	2.6	0.8
13.02.2016	15:06:23	1.7	1.7	1.4	39.4	256.2	57.7	3.5	0.4
03.08.2016	12:22:00	2	2.4	2.4	99.1	361	79.3	3.7	0.4
05.01.2017	21:56:50	1.8	2.2	2	68.7	403.1	90	3.5	0.7
24.02.2017	3:45:35	2.1	2.3	1.9	57.9	299	21	3.1	0.8
08.04.2017	14:20:09	1.7	1.7	1.3	29.7	313	60.1	3.2	0.8
18.07.2017	8:53:08	1.8	2	1.6	81.9	371.7	79.9	2.8	1.1
22.08.2017	5:27:19	2.1	2.5	1.4	32.5	394	67.7	8.4	1.2
06.05.2018	1:54:26	1.6	2.1	1.8	50.6	317.3	40	3.6	0.8
20.08.2018	8:11:47	1.8	1.8	1.2	35.9	308.6	69	2.8	0.8
24.09.2019	22:27:47	1.8	2.3	1.6	54.9	281.2	82.4	4.1	0.9
20.03.2021	11:16:59	2.1	3.1	2.2	105.3	303.2	30.8	3.2	1.2
15.07.2021	19:15:14	1.3	2.2	1.7	44.4	380.7	51.1	7.7	0.9
11.02.2022	22:06:14	1.9	2.3	1.7	84	392.4	58.9	4.9	1.1
25.03.2024	10:04:53	2.2	1.1	1.2	67.4	631.8	80.8	5.5	0.9

FIGURE CAPTIONS

Fig. 1. Types of interplanetary shock waves. *N, T, B, V* - concentration, temperature, magnetic field modulus, and solar wind velocity, respectively. The course of parameters for all types is presented on the time scale of registration on the spacecraft.

Fig. 2. Time course of parameters during the passage of the fast backward interplanetary FR shock wave on March 20, 2021: (*a*) plasma flux velocity; (*b*) proton temperature; (*c*) proton concentration; (*d*) MMP modulus; (*e*) MMP components (in GSE coordinates).

Fig. 3. Variation of solar wind plasma parameters during the passage of FR-type interplanetary shock waves (from left to right): interplanetary magnetic field modulus *B*; proton concentration *N*; proton temperature *T*; solar wind transport velocity *delta V* (difference of moduli values in the perturbed and undisturbed region). Index d is the perturbed region, u is the unperturbed region.

Fig. 4. Classifying plasma parameters of FR-type interplanetary shock waves (from left to right): V_{IP}- shock wave propagation velocity, θ_{Bn}- the angle between the normal to the MCE front and the magnetic field vector in the unperturbed region, M_{ms}- Mach magnetosonic number, β - beta parameter (ratio of thermal pressure to magnetic pressure in the unperturbed region).

Fig. 5. Fluctuation spectra of the components of the MMP interplanetary magnetic field for the reverse shock wave in the unperturbed region. From left to right, the following components are given: *Bx, By, Bz*, $B\parallel$, $B\perp$ to the MUV normal. The values of the slope indices of the spectrum *K* for the MHD and the transient part of the spectrum are indicated.

Fig. 6. Fluctuation spectra of the MMP interplanetary magnetic field components for the reverse shock wave in the perturbed region. From left to right, the following components are given: *Bx, By, Bz*, $B\parallel$, $B\perp$ to the MUV normal. The values of the slope indices of the spectrum *K* for the MHD and the transient part of the spectrum are indicated.

Fig. 7. Histograms of the distribution of the slopes of the spectra of backshock wave fluctuations in the MHD part of the spectrum for the unperturbed region (upper line) and for the perturbed (lower line) region of the solar wind.

Fig. 8. Histograms of the distribution of the slopes of the spectra of inverse shock wave fluctuations in the transient part of the spectrum for the unperturbed region (top row) and for the perturbed (bottom row) region of the solar wind.

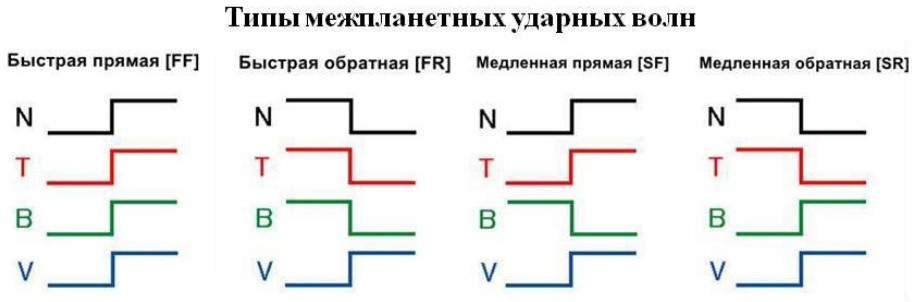
Типы межпланетных ударных волн
Быстрая прямая [FF]
Быстрая обратная [FR]
Медленная прямая [SF]
Медленная обратная [SR]
N
T
B
V

Fig. 1.

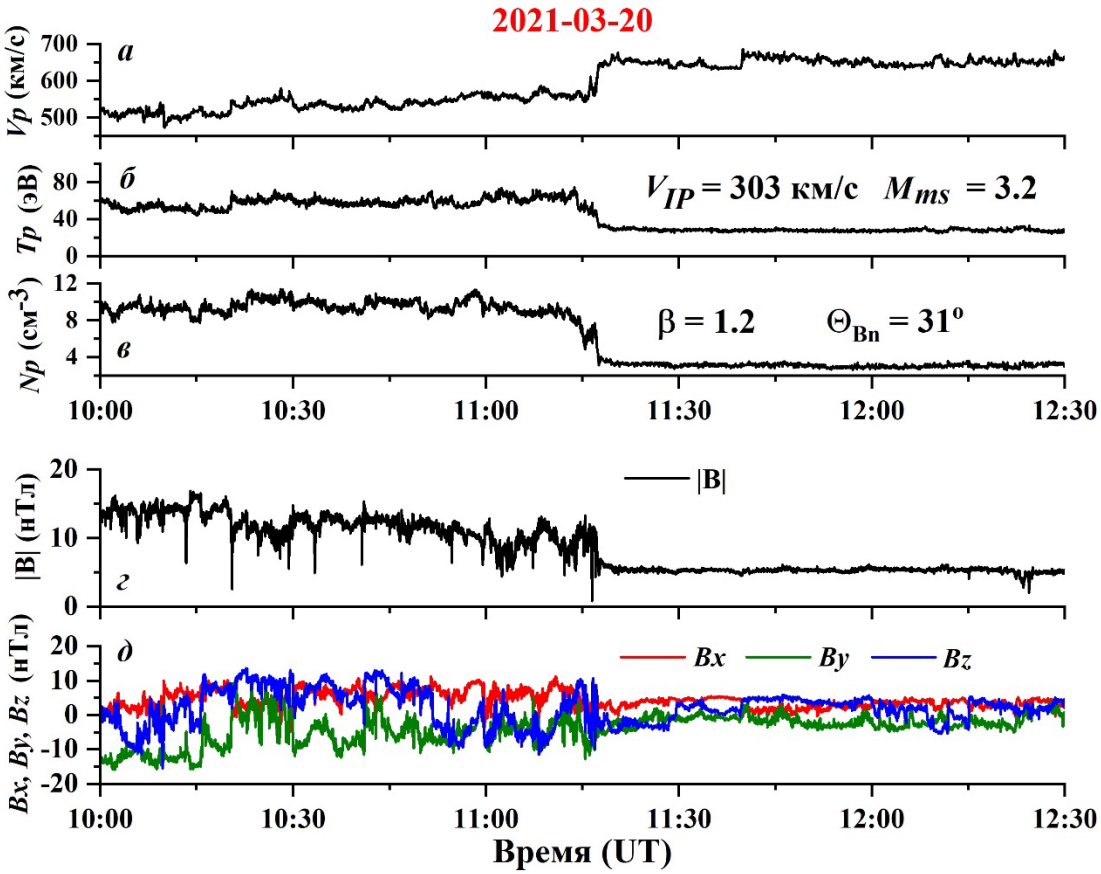
2021-03-20
Vp (км/с)
а
б
Tp (эВ)
Np (см-3)
в
VIP = 303 км/с Mms = 3.2
β = 1.2
ΘBn = 31°
|B| (нТл)
г
|B|
Bx, By, Bz (нТл)
д
Bx
By
Bz
10:00
10:30
11:00
11:30
12:00
12:30
Время (UT)

Fig. 2.

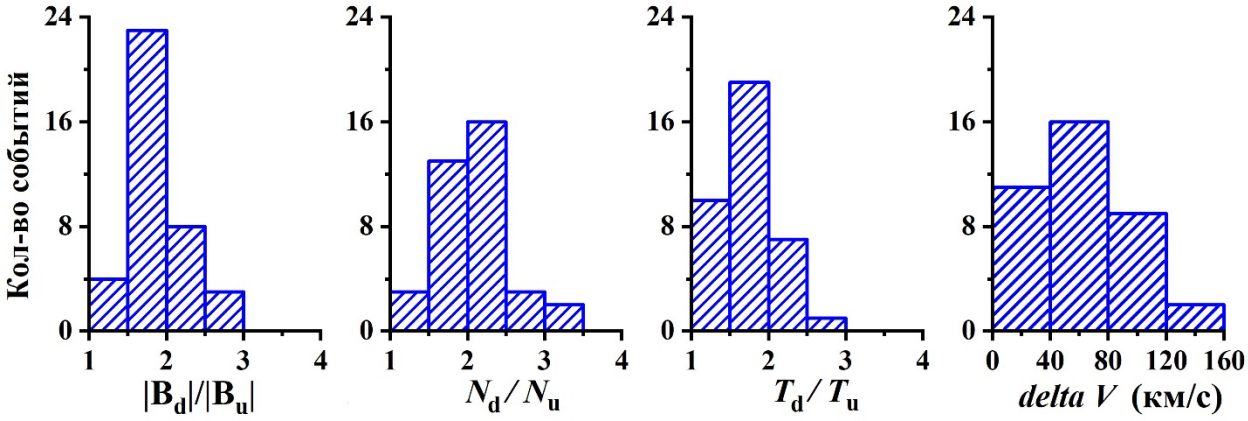
Кол-во событий
|Bd|/|Bu|
Nd / Nu
Td / Tu
delta V (км/с)

Fig. 3.

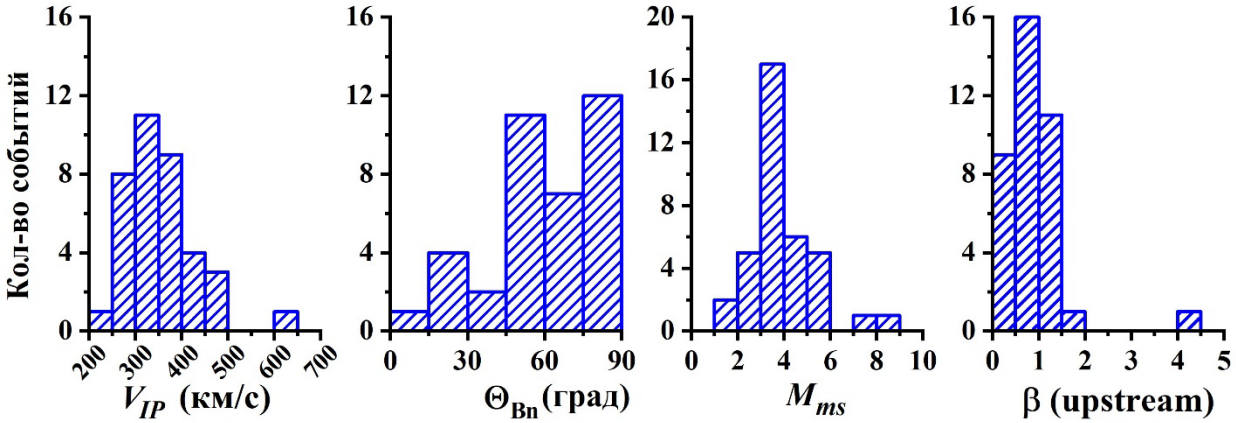
Кол-во событий
VIP (км/с)
ΘBn(град)
Mms
β (upstream)

Fig. 4.

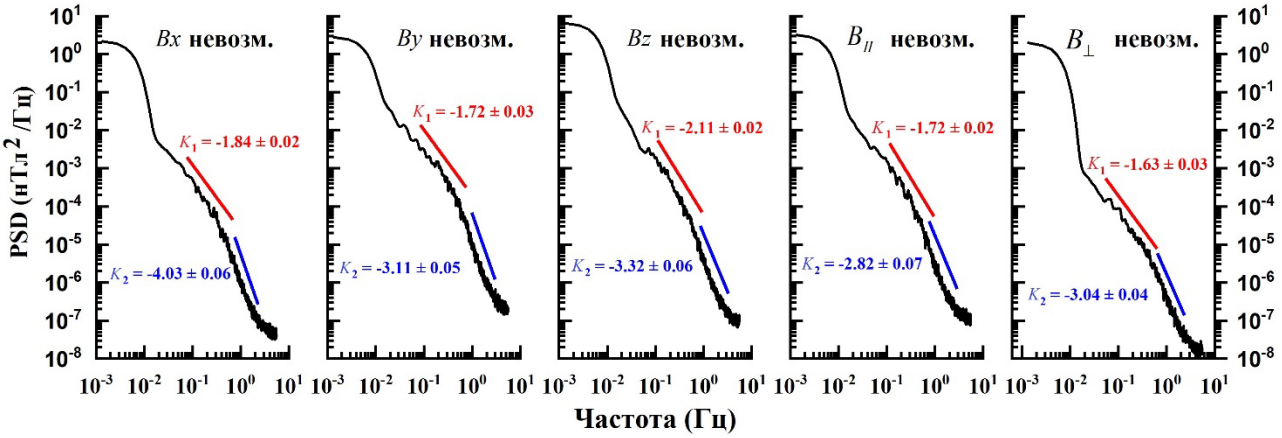
Bx невозм.
By невозм.
Bz невозм.
B// невозм.
B⊥ невозм.
K1 = -1.84 ± 0.02
K2 = -4.03 ± 0.06
K1 = -1.72 ± 0.03
K2 = -3.11 ± 0.05
K1 = -2.11 ± 0.02
K2 = -3.32 ± 0.06
K1 = -1.72 ± 0.02
K2 = -2.82 ± 0.07
K1 = -1.63 ± 0.03
K2 = -3.04 ± 0.04
PSD (нТл2/Гц)
Частота (Гц)

Fig. 5.

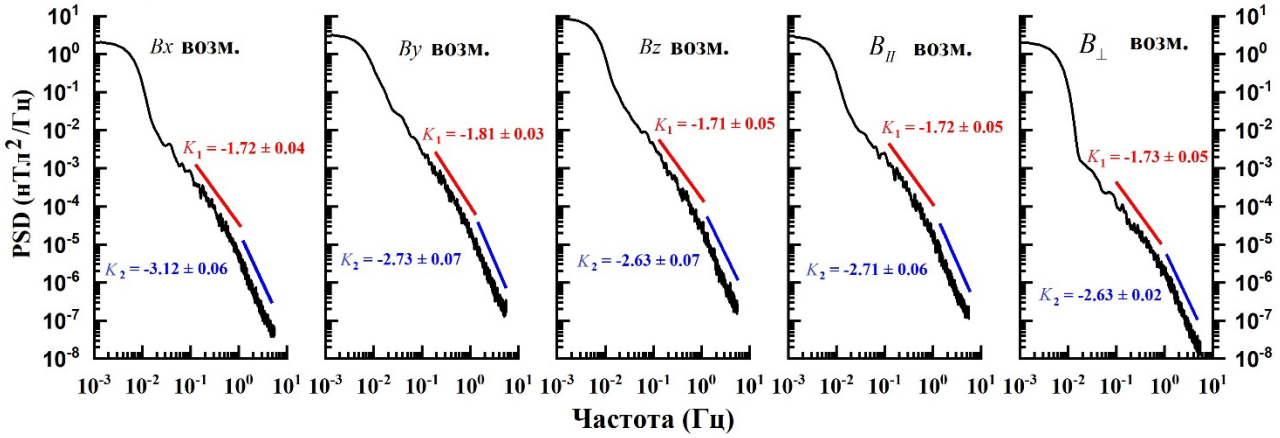
Bx возм.
By возм.
Bz возм.
B// возм.
B⊥ возм.
K1 = -1.72 ± 0.04
K2 = -3.12 ± 0.06
K1 = -1.81 ± 0.03
K2 = -2.73 ± 0.07
K1 = -1.71 ± 0.05
K2 = -2.63 ± 0.07
K1 = -1.72 ± 0.05
K2 = -2.71 ± 0.06
K1 = -1.73 ± 0.05
K2 = -2.63 ± 0.02
PSD (нТл2/Гц)
Частота (Гц)

Fig. 6.

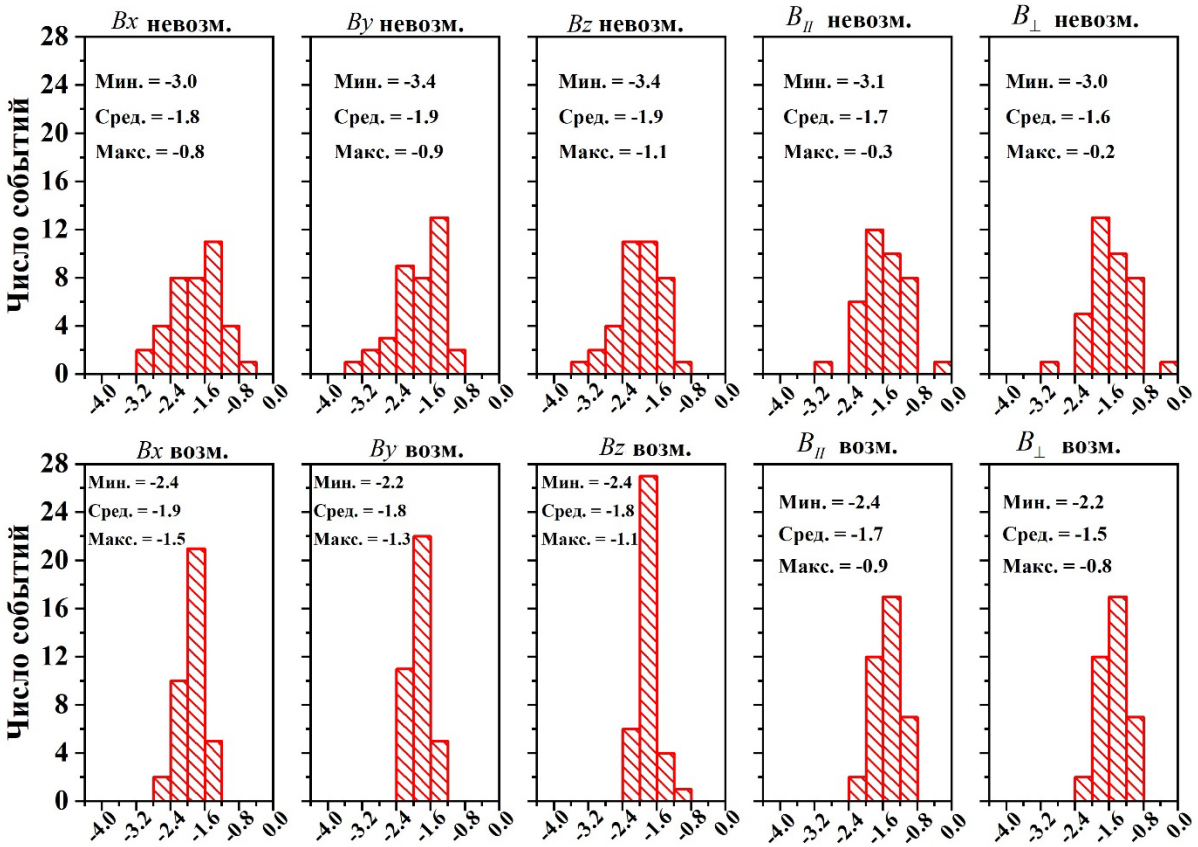
Bx невозм.
Мин. = -3.0
Сред. = -1.8
Макс. = -0.8
By невозм.
Мин. = -3.4
Сред. = -1.9
Макс. = -0.9
Bz невозм.
Мин. = -3.4
Сред. = -1.9
Макс. = -1.1
B// невозм.
Мин. = -3.1
Сред. = -1.7
Макс. = -0.3
B⊥ невозм.
Мин. = -3.0
Сред. = -1.6
Макс. = -0.2
Bx возм.
Мин. = -2.4
Сред. = -1.9
Макс. = -1.5
By возм.
Мин. = -2.2
Сред. = -1.8
Макс. = -1.3
Bz возм.
Мин. = -2.4
Сред. = -1.8
Макс. = -1.1
B// возм.
Мин. = -2.4
Сред. = -1.7
Макс. = -0.9
B⊥ возм.
Мин. = -2.2
Сред. = -1.5
Макс. = -0.8
Число событий
0
4
8
12
16
20
24
28
-4.0
-3.2
-2.4
-1.6
-0.8
0.0

Fig. 7.

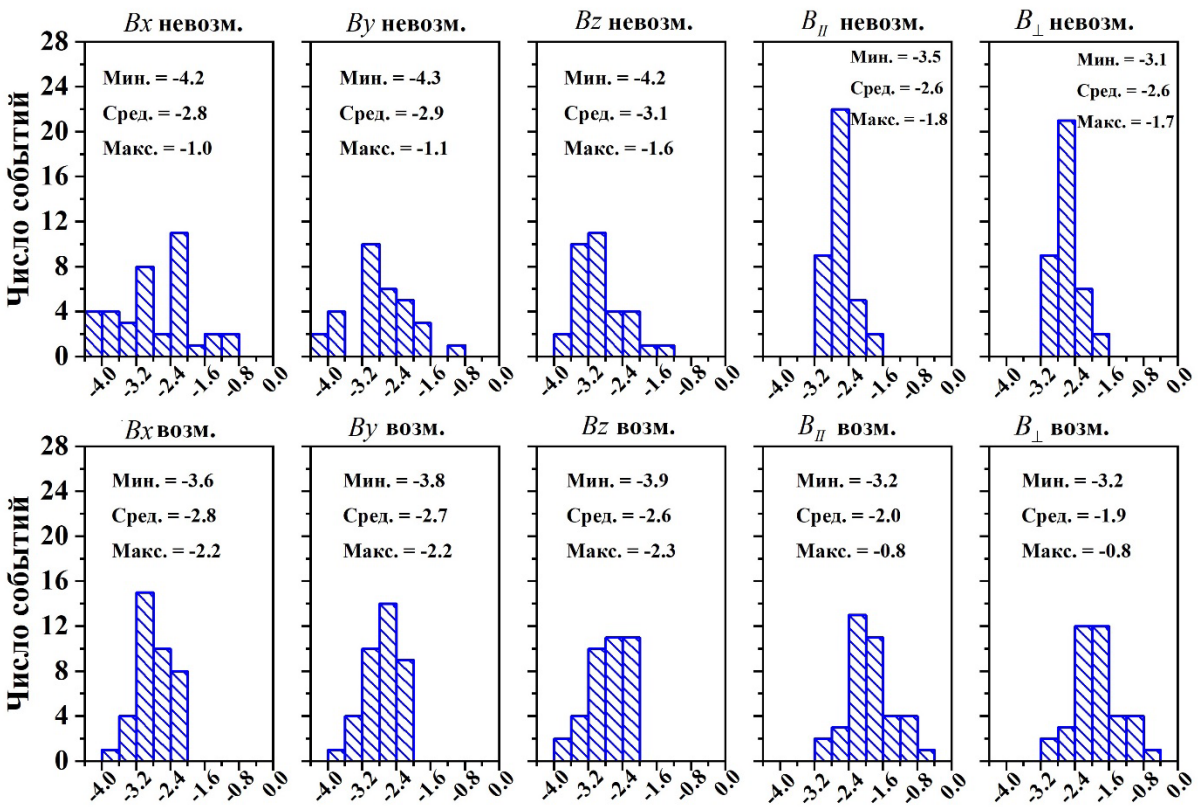
Bx невозм.
Мин. = -4.2
Сред. = -2.8
Макс. = -1.0
By невозм.
Мин. = -4.3
Сред. = -2.9
Макс. = -1.1
Bz невозм.
Мин. = -4.2
Сред. = -3.1
Макс. = -1.6
B|| невозм.
Мин. = -3.5
Сред. = -2.6
Макс. = -1.8
B⊥ невозм.
Мин. = -3.1
Сред. = -2.6
Макс. = -1.7
Bx возм.
Мин. = -3.6
Сред. = -2.8
Макс. = -2.2
By возм.
Мин. = -3.8
Сред. = -2.7
Макс. = -2.2
Bz возм.
Мин. = -3.9
Сред. = -2.6
Макс. = -2.3
B|| возм.
Мин. = -3.2
Сред. = -2.0
Макс. = -0.8
B⊥ возм.
Мин. = -3.2
Сред. = -1.9
Макс. = -0.8
Число событий
0
4
8
12
16
20
24
28
-4.0
-3.2
-2.4
-1.6
-0.8
0.0

Fig. 8.